# The Mn effect on magnetic structure of FeMn-B amorphous metals

Yang Wang[1], D.M.C. Nicholson[2], M. Widom[3], M. Fuentes-Cabrera[2,3], and M. Mihalkovic[3]
[1]Pittsburgh Supercomputing Center, Carnegie Mellon University, Pittsburgh, PA 15213
[2]Computational Physics Division, Oak Ridge National Laboratory, Oak Ridge, TN 37831
[3]Department of Physics, Carnegie Mellon University, Pittsburgh, PA 15213

## ABSTRACT

Fe-rich Fe-B amorphous metals exhibit approximately collinear magnetic structure. When a certain amount of Fe atoms are replaced with Mn, the magnetic structure of the alloys is found to become non-collinear. We performed electronic structure calculations using the locally self-consistent multiple scattering (LSMS) method for supercell samples generated by ab initio molecular dynamics simulation using the Vienna Ab-initio Simulation Package (VASP). We present the distribution of moment sizes and angular distributions in the FeMn-B amorphous metal samples. We discuss the Mn effect on the magnetic structure of the alloys.

## INTRODUCTION

Amorphous metals, also known as metallic glasses, differ from ordinary metals in that their constituent atoms are not arranged on a crystalline lattice. Because of this, they exhibit unique combination of physical properties [1,2]. Until recently, they have largely been manufactured in the form of thin ribbons usually less than 1mm in thickness, because fast cooling rate is (~ $10^6$ ˚K/sec) required for retaining the metastable amorphous phase. In contrast, the bulk amorphous metals are made with conventional cooling methods. Since they were firstly discovered in the early 1980s [3,4], the bulk amorphous metals have attracted much attention from researchers for their properties such as low volume shrinkage, high mechanical strength and hardness, low surface roughness, and possibly high resistance to corrosions. (See reference [5] for a historical summary on the discovery of bulk amorphous metals.) They have been proposed for a range of potential applications in sporting goods materials, medical and dental implants, machining tools, coatings, and more. Recently, a number of Fe-based bulk amorphous metals have been made in laboratory. In addition to the mechanical properties we just mentioned, they show some unique magnetic properties such as high saturation magnetization and high permeability, which make them a good candidate for magnetic core materials in transformers and electrical motors. Lately, high Mn content, Fe-based bulk amorphous metals have been investigated by Poon *et al* as prospective amorphous steels [6]. These are nonmagnetic structural amorphous metals with magnetic transition temperatures far below the ambient temperature.

To understand the Mn effect on the magnetic structure of Fe-based amorphous metals, we carried out theoretical investigation of the $Fe_{0.8-x}Mn_xB_{0.2}$ alloys using *ab initio* electronic structure calculation techniques. We determined the magnetic structure of the alloys for Mn contents ranging from 0 to 80 percent. A detailed description of our theoretical approach is given in the following section.

## THEORETICAL APPROACH

We start with a 100-atom unit cell sample that models a $Fe_{0.8}B_{0.2}$ amorphous alloy. The unit cell sample contains 80 Fe atoms and 20 B atoms and repeats itself to fill the entire space. The structure of the unit cell sample is obtained by a quenching process that starts from a high temperature, where the sample is in liquid state, to a low temperature, where the sample is in its amorphous solid state. In our approach, the atomic movement during the quenching process is determined by molecular dynamics simulation using the Vienna *Ab-initio* Simulation Program (VASP) [7]. After the $Fe_{0.8}B_{0.2}$ amorphous alloy sample is constructed, we select randomly a certain number of Fe atoms in the unit cell and replace them with Mn atoms to obtain a $Fe_{0.8-x}Mn_xB_{0.2}$ amorphous alloy sample.

Given the unit cell sample that models the amorphous structure of $Fe_{0.8-x}Mn_xB_{0.2}$ amorphous alloys, we apply the locally self-consistent multiple scattering (LSMS) method [8] to calculate the electronic and magnetic structures of the alloys. The LSMS method is an order-N approach to the *ab-initio* electronic structure calculation. By order-N, we mean that the computational effort of the LSMS method scales linearly with respect to the number of atoms in the unit cell, rather than cubically like most other *ab-initio* methods. Using the LSMS method, we can study both collinear and the non-collinear magnetic states of the alloys. Specifically, we apply the spin-polarized LSMS calculation to the collinear magnetic state and apply spin-canted LSMS calculation to the non-collinear magnetic state. In the spin-polarized calculation, the magnetic moment on each atom is constrained along a predefined direction, usually z-axis. In the spin-canted calculation, the moment orientation is not restricted, and the ground state magnetic structure is obtained from *ab-initio* spin dynamics simulation [9], in which the magnetic moment orientation on each atom allows to change under the influence of a local effective magnetic field and is treated as a classical spin that satisfies a Landau-Lifshitz-Gilbert equation [10,11]. The local effective magnetic field is the summation of the local exchange field resulting from the local spin density approximation [12] to the density functional theory [13,14] and the local transverse constraining field which is necessary for maintaining the orientation of the local moments unchanged between each time step while we are searching for the electronic ground state associated with the given magnetic moment configuration. The spin dynamics simulation starts with a random distribution of atomic moment orientation, evolves as the atomic moments rotate under the influence of a local effective magnetic field, and ends when the final ground state is reached. In the final ground state, the constraining field acting on each atom is zero and the local exchange field is collinear with the local magnetization orientation. A detailed description of the LSMS method, the spin-dynamics simulation algorithm, and its application to the study of the electronic and magnetic structure of Fe-based amorphous alloys can be found in our previous publications [8,9,15,16].

## RESULTS

We performed spin-polarized and spin-canted LSMS calculations for $Fe_{0.8}B_{0.2}$, $Fe_{0.7}Mn_{0.1}B_{0.2}$, $Fe_{0.6}Mn_{0.2}B_{0.2}$, $Fe_{0.5}Mn_{0.3}B_{0.2}$, $Fe_{0.4}Mn_{0.4}B_{0.2}$, $Fe_{0.3}Mn_{0.5}B_{0.2}$, $Fe_{0.2}Mn_{0.6}B_{0.2}$ , $Fe_{0.1}Mn_{0.7}B_{0.2}$, and $Mn_{0.8}B_{0.2}$ unit cell samples. The energy difference between the spin-cant and the spin-polarized calculations for these samples is plotted in figure 1. Note that the spin-polarized calculation intrinsically sets the limitation on the electronic state space, and as a result, the corresponding

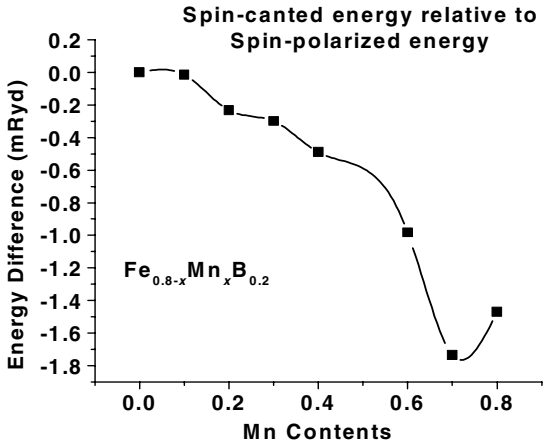


Figure 1. Total energy difference (in mRyd) per atom between the spin-canted and the spin-polarized calculations versus Mn content for $Fe_{0.8-x}Mn_xB_{0.2}$ amorphous alloy samples.

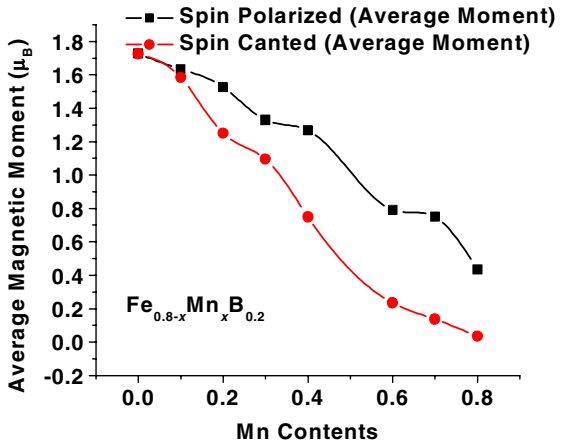


Figure 2. Average magnetic moment (in $\mu_B$) per atom from the spin-canted and the spin-polarized calculations versus Mn content for $Fe_{0.8-x}Mn_xB_{0.2}$ amorphous alloy samples.

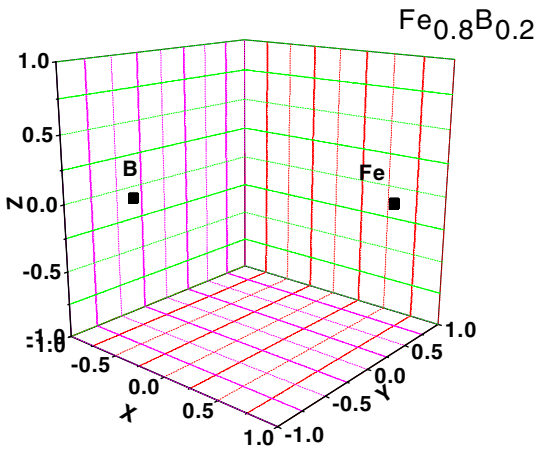


Figure 3(a). $Fe_{0.8}B_{0.20}$: Magnetic moment orientation in the sample.

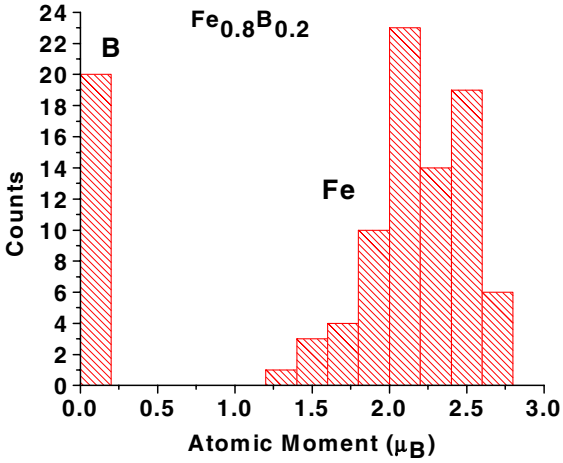


Figure 3(b). $Fe_{0.8}B_{0.20}$: Magnetic moment distribution in the sample.

collinear magnetic structure is usually unrelaxed. As what we have expected, figure 1 shows that the total energy of the non-collinear magnetic state is lower than that of the collinear state. The average magnetic moment per atom versus the Mn content of the alloy samples is plotted in figure 2, where the spin-canted results are shown by solid circles and the spin-polarized results are shown by solid squares.

Obviously, as the Mn content increases, the average magnetic moment of the $Fe_{0.8-x}Mn_xB_{0.2}$ amorphous alloy sample decreases. An illustrative description for the magnetic structure of $Fe_{0.8}B_{0.2}$, $Fe_{0.4}Mn_{0.4}B_{0.2}$, and $Mn_{0.8}B_{0.2}$ is shown in figure 3 (a and b), figure 4 (a and b), and figure 5 (a and b), respectively.

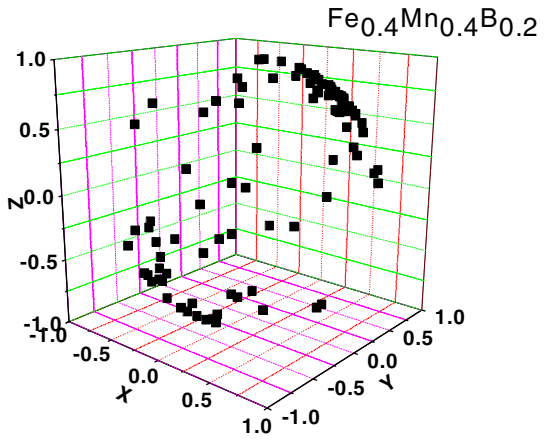


Figure 4(a). $Fe_{0.4}Mn_{0.4}B_{0.2}$: Magnetic moment orientation in the sample.

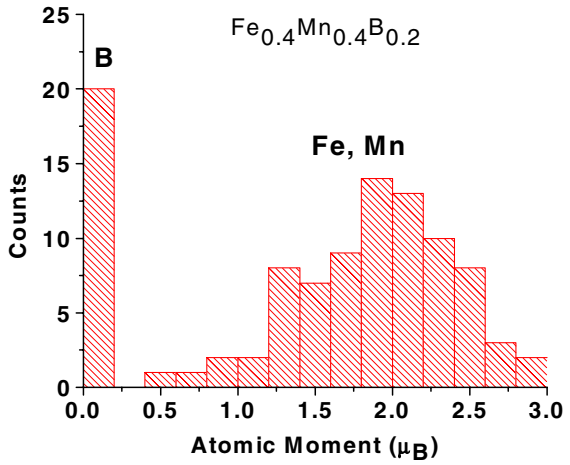


Figure 4(b). $Fe_{0.4}Mn_{0.4}B_{0.2}$: Magnetic moment distribution in the sample.

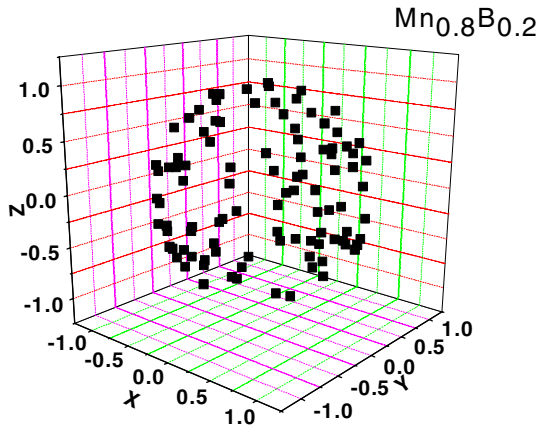


Figure 5(a). $Mn_{0.8}B_{0.2}$: Magnetic moment orientation in the sample.

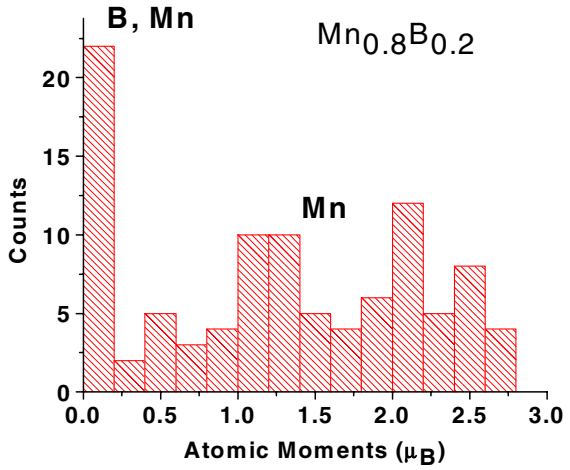


Figure 5(b). $Mn_{0.8}B_{0.2}$: Magnetic moment distribution in the sample.

## DISCUSSIONS AND CONCLUSIONS

In the previous section, we presented the calculated results for $Fe_{0.8-x}Mn_xB_{0.2}$ amorphous alloys. In particular, we showed the magnetic structure of $Fe_{0.8}B_{0.2}$, $Fe_{0.4}Mn_{0.4}B_{0.2}$, and $Mn_{0.8}B_{0.2}$ alloy samples. We noted that the non-collinear magnetic state has lower energy than the collinear state. Evidently, the energy difference between the two magnetic states becomes more dramatic as Mn content increases and can reach as big as 1.8 mRyd. This reveals that the non-collinear magnetic structure in FeMn-based amorphous alloys on Mn-rich side is significant and its contribution to the energetic of the alloys should not be ignored.

Without Mn atoms being present, $Fe_{0.8}B_{0.2}$ is essentially collinear. This is evident from the energy plot (Fig. 1) and the average moment plot (Fig. 2), where at zero Mn content the spin-polarized and the spin-canted calculations give approximately the same total energy and the same average magnetic moment. A detailed picture for the magnetic structure of $Fe_{0.8}B_{0.2}$ is shown in Fig. 3(a) and Fig. 3(b). Fig. 3(a) reveals that all Fe moments are pointing in one direction and all B moment are pointing in a direction that is opposite to the Fe moments. The B moment is small compared to the Fe moment while the Fe moment varies from site to site, ranging from $1.25\mu_B$ to $2.8\mu_B$. This reveals that the magnetic structure of $Fe_{0.8}B_{0.2}$, even though collinear, is rather more complicated than a simple ferromagnetic picture.

As Mn content increases, the average magnetic moment decreases as shown in Fig. 2, and the non-collinear magnetic structure of $Fe_{0.8-x}Mn_xB_{0.2}$ becomes more evident. Both Fig. 4(a) and Fig. 4(b) show that the distribution of the individual moment orientation and magnitude becomes widely spread. The B moments remain to be small, and the Fe and the Mn moments vary from $0.4\mu_B$ to $3.0\mu_B$.

As Mn content approaches to its maximum value, the average magnetic moment of $Mn_{0.8}B_{0.2}$ amorphous alloy is suppressed, and the alloy sample becomes paramagnetic. The individual moment orientation showed in Fig. 5(a) reveals a more uniform distribution in space than the one shown in Fig. 4(a) that indicates a spin glass type magnetic structure. Even though the magnetic moment of the entire sample cease to exist, the size of individual Mn moments in the sample is rather significant, ranging from $0.1\mu_B$ to $2.8\mu_B$.

Finally, we note that the energy difference between the non-collinear and collinear states is not monotonically increasing as Mn content increases. There is a sudden change in the trend when Mn content is reaching 80 percent. This can be simply attributed to the sample configuration effect, where different way of replacing Fe atoms with Mn atoms makes somewhat different energy contributions. This sample configuration effect will be reduced to minimum by self-averaging when rather larger unit cell samples are used. For the present study, the unit cell sample size is 100 atoms, due to the computational limitation of VASP. We are hoping to achieve better statistics to improve our spin dynamics calculation by going beyond 100 atoms per unit cell limit. To generate larger $Fe_{0.8-x}Mn_xB_{0.2}$ unit cell samples, we plan to use our EAM based semi-empirical molecular dynamics simulation technique, which is described in the paper by Miguel Fuentes-Cabrera *et al* in the current proceeding [17].

## ACKNOWLEDGMENTS

The authors thank their colleagues J. Poon, T. Egami, D. Louca, and G. Shiflet for helpful discussions. The research is supported by DARPA/ONR Grant N00014-01-1-0961. The VASP and LSMS calculations were performed at Pittsburgh Supercomputing Center and NERSC.

## REFERENCES

1. See articles in *Amorphous Metallic Alloys*, edited by F.E. Luborsky, (Butterworths, London, 1983).
2. R.W. Cahn, in *Glasses and Amorphous Materials*, edited by J. Zarzycki, (Mater. Sci. Tech. **9**, VCH Press, Weinheim, 1991) pp. 493-548.
3. H.W. Kui, A.L. Greer, and Turnbull, *Appl. Phys. Lett*. **45**, 615 (1984).
4. A.J. Drehman and A.L. Greer, *Acta. Metall.* **32**, 323 (1984).
5. A. Inoue, *Mater. Sci. Eng*. **A304-306**, 1 (2001).
6. S.J. Poon, G.J. Shiflet, V. Ponnambalam, V.M. Keppens, R. Taylor, and G. Petculescu, in *Supercooled Liquids, Glass Transition and Bulk Metallic Glasses*, edited by T. Egami, A.L. Greer, A. Inoue, and S. Ranganathan, (Mater. Res. Soc. Proc. 754, Warrendale, PA, 2003,) pp. 167-177.
7. http://cms.mpi.univie.ac.at/vasp/vasp/vasp.html.
8. Y. Wang, G.M. Stocks, W.A. Shelton, D.M.C. Nicholson, W.M. Temmerman, and Z. Szotek, *Phys. Rev. Lett*. **75**, 2867 (1995).
9. G.M. Stocks, B. Ujfalussy, X. Wang, D.M.C. Nicholson, W.A. Shelton, Y. Wang, A. Canning, and B.L. Gyorffy, *Phil. Mag. B* **78**, 665 (1998).
10. L. Landau and E. Lifshitz, *Phys. Z. Sowjet*. **8**, 153 (1935).
11. T.L. Gilbert, *Phys. Rev*. **100**, 1243 (1955).
12. U. von Barth and L. Hedin, *J. Phys. C.* **5**, 1629 (1972).
13. W. Kohn and L.J. Sham, *Phys. Rev. A* **140**, 1133 (1965).
14. P.C. Hohenberg and W. Kohn, *Phys. Rev. B* **136**, 864 (1964).
15. Yang Wang, Mike Widom, Don Nicholson, Marek Mihalkovic, and Siddartha Naidu, in *Supercooled Liquids, Glass Transition and Bulk Metallic Glasses*, edited by T. Egami, A.L. Greer, A. Inoue, and S. Ranganathan, (Mater. Res. Soc. Proc. 754, Warrendale, PA, 2003,) pp. 439-444.
16. D.M.C. Nicholson, Yang Wang, and Mike Widom, in *Supercooled Liquids, Glass Transition and Bulk Metallic Glasses*, edited by T. Egami, A.L. Greer, A. Inoue, and S. Ranganathan, (Mater. Res. Soc. Proc. 754, Warrendale, PA, 2003,) pp. 451-456.
17. Miguel Fuentes-Cabrera, Don Nicholson, Mike Widom, Yang Wang, and Marek Mihalkovic (to be published in MRS proceeding.)